PAPER

The effect of local dissociation on dynamics of interacting molecular motors

IOP Publishing Journal of Physics A: Mathematical and Theoretical

J. Phys. A: Math. Theor. **52** (2019) 365001 (18pp) https://doi.org/10.1088/1751-8121/ab35bb

The effect of local dissociation on dynamics of interacting molecular motors

Luiza Gomes[1], Tripti Midha[2], Arvind Kumar Gupta[2] and Anatoly B Kolomeisky[1]

[1] Department of Chemistry and Department of Chemical and Biomolecular Engineering, Rice University, Houston, TX 77005, United States of America
[2] Department of Mathematics, Indian Institute of Technology Ropar, Rupnagar-140001, India

E-mail: tolya@rice.edu

Received 26 February 2019, revised 4 July 2019
Accepted for publication 25 July 2019
Published 13 August 2019

Abstract

Successful functioning of all living systems depends on several classes of active enzymatic molecules known as biological molecular motors. They are involved in processes that require the application of mechanical forces such as cellular transport, muscle functioning, synthesis of proteins and nucleic acids and many others. Experimental studies suggest that most biological molecular motors function collectively by interacting with each other and moving along linear tracks, from which they occasionally dissociate at specific locations. We develop a theoretical model to investigate the multi-particle dynamics of interacting molecular motors with local dissociations. It is specifically stimulated by ribosomes motion along ribonucleic acid (RNA) molecules during the protein synthesis when the ribosome complex might dissociate into the solution by encountering a specially localized region on RNA. In our theoretical approach, we model the dynamics of molecular motors as one-dimensional totally asymmetric simple exclusion processes for interacting particles. Using a cluster mean-field approach, which partially takes into account the correlations in the system, stationary properties such as particle currents, densities and phase diagrams are explicitly calculated. It is found that the presence of local dissociations increases the number of possible stationary phases. Furthermore, the strength of interactions between molecular motors, the modification of transition rates due to interactions and the frequency of dissociations strongly influence the dynamics of molecular motors. The microscopic origin of these observations are discussed. Our theoretical predictions are fully supported by Monte Carlo computer simulations.

Keywords: molecular motors, asymmetric exclusion processes, inter-molecular interactions

(Some figures may appear in colour only in the online journal)

1. Introduction

Several classes of active biological molecules, which are called motor proteins or molecular motors, are crucial for supporting various activities in all living organisms [1, 2]. These are enzymatic molecules that convert the chemical energy into mechanical work in order to support cellular processes that require the application of forces and torques [3]. They play important roles in a variety of biological processes, including cellular transport, muscles activity, maintaining and transfer of genetic information, protein synthesis and signaling [1, 2, 4–6]. Significant advances in our understanding of the microscopic mechanisms of biological molecular motors have been achieved [3, 6, 7]. However, many aspects of their dynamic behavior and related cellular functions remain not well explained [3, 7–9].

It is known that biological molecular motors support their activities by catalyzing several exothermic processes such as the hydrolysis of adenosine triphosphate (ATP) or biopolymerization [3]. They are capable of transforming a fraction of the released chemical energy into mechanical forces. Most molecular motors move along linear tracks such as cytoskeleton protein filaments or nucleic acids, from which they might occasionally dissociate into the cellular solution. A large number of motor proteins function collectively by working in groups of various sizes [3, 9, 10]. Experiments suggest that many molecular motors interact with each other [11, 12]. This could be direct chemical interactions due to being spatially close on molecular filaments, or it might be indirect effective interactions due to the influence of the linear tracks on which the motors move. An interesting example of biological molecular motors that exhibit all these features is a protein synthesis by ribosomes that translocate along ribonucleic acid (RNA) molecules [13]. Several ribosome molecules simultaneously move along the same RNA chain, which sometimes leads to traffic jams on RNA chains. There are also certain regions on RNA where ribosome has a higher probability to detach from the track, terminating the protein synthesis process [13].

Several theoretical approaches have been proposed to investigate the properties of biological molecular motors [3–6, 14]. Totally asymmetric simple exclusion processes (TASEP) are multi-particle non-equilibrium models that have been widely employed to describe the collective dynamics of molecular motors [6, 15–25]. The molecular transport on parallel linear tracks, the impact of local dissociations, and the effect of the motors sizes have been successfully studied using this approach. Stimulated by experimental observations that motor proteins interact beyond simple exclusion [11, 12], we recently developed a new class of TASEP models that takes into account inter-molecular interactions via a thermodynamically consistent approach [18–21]. It was shown that these interactions strongly influence the dynamics of molecular motors.

In this work, we investigate a theoretical model, based on TASEP, that takes into account two important features of biological molecular motors: interactions and local dissociations. It is specifically motivated by the protein synthesis process that is accomplished by the ribosome molecular motors. A situation with a single dissociation site far away from the boundaries of the system is specifically considered in our analysis. It is argued that the dissociation site divides the linear track into two homogeneous segments, for which theoretical results are known. We develop a cluster mean-field approach to analyze the behavior of molecular motors

by properly coupling the multi-particle dynamics in both parts of the system. Inter-molecular interactions are described in the thermodynamically consistent fashion. This approach partially takes into account the correlations between particles, which is a crucial feature for studying one-dimensional multi-particle processes. Our theoretical analysis identifies several dynamic phases and it shows how varying the interactions strength, the effect of interactions on transition rates and the possibility of dissociations modify the dynamic properties of biological molecular motors. We supplement our analytical calculations with extensive Monte Carlo computer simulations, which fully support all theoretical predictions.

2. Theoretical model

2.1. Model description

Our goal is to investigate the dynamics of interacting molecular motors that also can dissociate from the linear track at some specific locations. We consider a lattice consisting of N sites that corresponds to a linear track on which the molecular motors translocate only in one direction: from left to right (see figure 1). Molecular motors are represented by particles in the system. They can enter the system only at the first site (if it is not occupied), and they can exit the system at the last site: see figure 1(A). Each site can only be in one of the two possible states, occupied or empty, and two particles cannot occupy the same site. This reflects the hard-core exclusion contribution in the inter-molecular interactions.

Particles located at the two neighboring sites also interact with each other, creating an effective inter-molecular bond, and we associate an energy E (in $k_{\mathrm{B}}T$ units) with the strength of this bond. Attractive interactions correspond to $E > 0$, while for the repulsive interactions we have $E < 0$. These nearest-neighbor interactions are affecting all transition rates in the system. We assume that the molecule hops along the lattice one step to the right if this site is available. The stepping transition is q if a new inter-molecular bond is made, or the rate is r if the inter-molecular bond is broken (figure 1(A)). For all other situations when the number of inter-molecular bonds does not change, the stepping rate is taken to be equal to 1: see figure 1(A).

The important part of our theoretical method is that the effect of inter-molecular interactions on transition rates is taken into account in the thermodynamically consistent way [18–21]. More specifically, the stepping rates can be written as

$$q = \exp\left[\theta E\right], \quad r = \exp[(\theta - 1)E], \tag{1}$$

where a parameter $0 \leqslant \theta \leqslant 1$ describes how the interaction influences the bond-making and the bond-breaking transitions. If there are no interactions, $E = 0$, we have $q = r = 1$. Generally, the transition rates q and r are related to each other via a detailed-balance like relation,

$$\frac{q}{r} = \exp(E). \tag{2}$$

The physical meaning of equations (1) and (2) is the following. If making the inter-molecular bond is energetically favorable ($E > 0$), then the forward stepping that is associated with the bond creation is fast ($q > 1$), while the stepping that leads to the bond breaking is slow ($r < 1$). But if the formation of the bond is energetically unfavorable ($E < 0$), then the forward stepping associated with the bond creation is slow ($q < 1$), while the motion that leads to the bond dissociation is fast ($r > 1$).

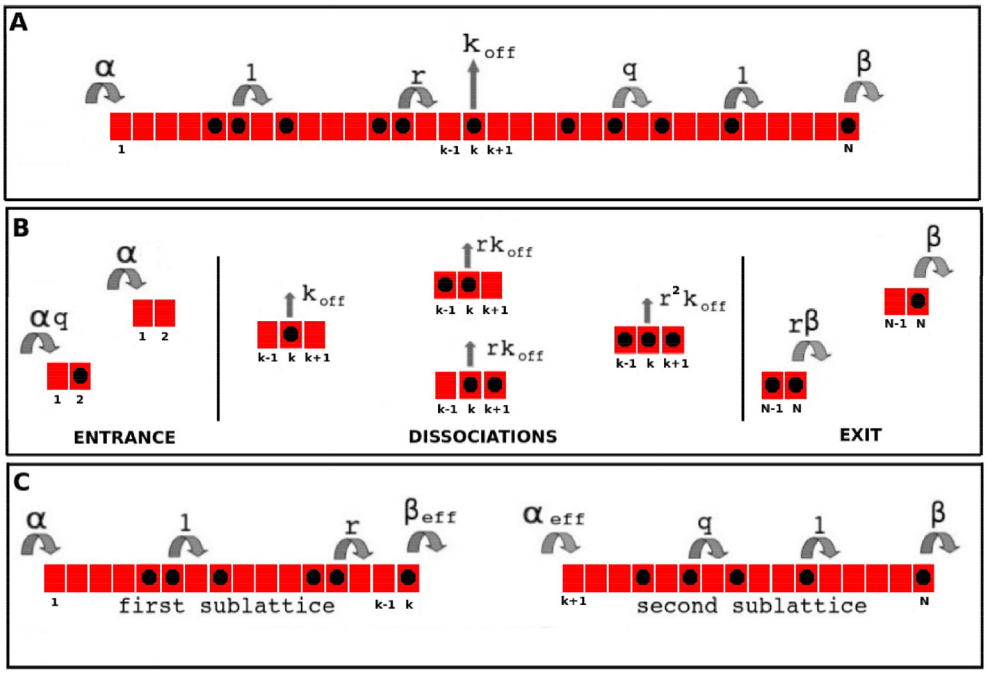

Figure 1. (A) A schematic view of the model of interacting molecular motors moving along linear filaments with a possibility of local dissociation. (B) Dynamic transitions at the entrance site, at the dissociation site and at the exit site. (C) Mapping of the original model into two coupled homogeneous sub-lattices.

Interactions are also affecting the entrance and exit transition rates. The particle enter the system at the site $i = 1$ with a rate α if the site $i = 2$ is empty (figure 1(B)). But if the second site is already occupied, the entrance rate is $q\alpha$ because the new inter-molecular bond will be created. Similarly, the particle at the last site ($i = N$) will leave the system with a rate β if there is no other particle at the site $i = N - 1$, as shown in figure 1(B). But when the site $i = N - 1$ is occupied the exit rate is equal to $r\beta$ because it will lead to the breaking of the inter-molecular bond.

To describe the effect of localized dissociations, we assume that there is a single site $1 < k < N$ far away from the boundaries from which the particle can irreversibly dissociate into the solution and leave the system. The exact location of the dissociation site is not important in the thermodynamic limit that we are interested in this work ($N \gg 1$), as long as this special location is far away from both boundaries. Clearly, interactions influence the dissociation rates from this special site. The nearest-neighbor interactions at site $i = k$ lead to three possible situations: see figure 1(B). If there are no other particles at the sites $i = k - 1$ and $i = k + 1$ then the dissociation rate is equal to $k_{\rm off}$. If only one of the sites neighboring to the special location is occupied ($i = k - 1$ or $i = k + 1$), then the dissociation rate is $rk_{\rm off}$. This is because in this case the particle dissociation will break only one inter-molecular bond. If both neighboring sites are occupied then the dissociation rate is given by $r^2k_{\rm off}$ to reflect the fact that the dissociation in this case will break two inter-molecular bonds.

The stationary properties of TASEP models can be successfully analyzed using exact or approximate approaches if the dynamics in the bulk is homogeneous [15]. But in our system the existence of the local dissociation site makes the system inhomogeneous, and because

of this the analysis using known methods that work for homogeneous systems is not possible. However, one might notice that the dissociation site divides the system into two homogeneous segments: L_1—from $i = 1$ to $i = k$ and L_2—from $i = k + 1$ to $i = N$, as shown in figures 1(A) and (C). The effective exit rate from the first segment is given by β_{eff}, and the effective entrance rate into the second sub-lattice is equal to α_{eff} (figure 1(C)). Then we might employ the results of homogeneous TASEP methods for calculating the dynamic properties at each sub-lattice separately, and the stationary arguments could be utilized to couple both parts of the system by explicitly evaluating the effective rates α_{eff} and β_{eff}. This is the main idea of our theoretical method for investigating the non-equilibrium dynamics of multiple interacting particles with the local dissociation.

2.2. Dynamic properties for homogeneous TASEP model of interacting particles

To calculate the dynamic properties in our model, we need to use the results for a homogeneous TASEP model of interacting particles. It was shown before that a satisfactory description of this model can be obtained by employing a cluster mean-field approach that partially takes into account the correlations in the system [18–21]. In this approach, the dynamics inside the cluster of several lattice sites is accounted for explicitly while the correlations between clusters are neglected.

Let us consider a two-site cluster mean-field method that was utilized for specific calculations [20, 21]. In this method, every two lattice sites, i and $i + 1$, can be found in one of four possible states: $(1, 1)$ when particles are found at both sites i and $i + 1$, $(1, 0)$ when only the site i is occupied, $(0, 1)$ when only the site $i + 1$ is occupied, and $(0, 0)$ when both sites are empty. The corresponding probabilities for each state can be written as $P(1, 1)$, $P(1, 0)$, $P(0, 1)$ and $P(0, 0)$, and they are related to each other via the normalization,

$$P(1,1) + P(1,0) + P(0,1) + P(0,0) = 1. \tag{3}$$

It was found also that these probabilities are explicitly given by [20, 21]

$$P(1,1) \equiv x = \rho + \frac{r - \sqrt{r(r + 4(q - r)\rho(1 - \rho))}}{2(q - r)}; \tag{4}$$

$$P(1,0) = P(0,1) \equiv y = \frac{-r + \sqrt{r(r + 4(q - r)\rho(1 - \rho))}}{2(q - r)}; \tag{5}$$

$$P(0,0) \equiv z = (1 - \rho) + \frac{r - \sqrt{r(r + 4(q - r)\rho(1 - \rho))}}{2(q - r)}, \tag{6}$$

where $\rho = P(1, 1) + P(1, 0) = x + y$ is the single-site bulk density. The particle flux through the bulk of the system can be conveniently written in terms of these cluster probabilities,

$$J_{\text{bulk}} = \frac{y^2 z + q y^3 + r x y z + x y^2}{\rho(1 - \rho)}. \tag{7}$$

Theoretical calculations show that there are three stationary phases in the TASEP model of interacting particles [18–21]. If dynamics is governed by the entrance into the lattice then a low-density (LD) phase will occupy the system. For the case when exiting from the lattice is the rate-limiting step, we have a high-density (HD) phase. If bulk processes control the dynamics, the system will be found in a maximal-current (MC) phase.

Density profiles, particle currents and boundaries between different stationary phases can be explicitly calculated using the cluster mean-field approach. In the LD phase, the entrance particle current is given as [20]

$$J_{\mathrm{LD}} = \alpha(z + qy). \tag{8}$$

Because of the stationarity, the bulk current must be the same as the entrance current, $J_{\mathrm{bulk}} = J_{\mathrm{LD}}$, and from equations (7) and (8) we obtain the expression

$$\alpha = \frac{(r - C_1)\left[C_1(-r + q(2r-1)) + r\left[q + r - 2qr + 4(1-q)(q-r)\rho(1-\rho)\right]\right]}{2(q-r)^2(\rho-1)\rho\left[r - 2r\rho + C_1 + q(r - 2 + 2\rho - C_1)\right]}, \tag{9}$$

with

$$C_1 = \sqrt{r\left[r(1-2\rho)^2 - 4q(\rho-1)\rho\right]}. \tag{10}$$

This allows us to evaluate explicitly the bulk density in the LD phase ($\rho_{\mathrm{LD}} = \rho(\alpha)$) and the stationary particle flux. For example, in the case of no interaction ($E = 0$), it leads to $C_1 = 1$ and $\rho_{\mathrm{LD}} = \alpha$. For very strong repulsions ($E \to -\infty$), it can be shown that $C_1 \simeq r(1-2\rho)$ and $\rho_{\mathrm{LD}} = \alpha/(1+\alpha)$ [20, 21].

However, the density at the last site $i = N$ is not the same as the bulk density, and it can be found using the following arguments. The exit current can be written in terms of the cluster densities at the last two sites,

$$J_{\mathrm{exit},N} = \beta P_N(0,1) + r\beta P_N(1,1) = \beta\rho_N + \beta(r-1)P_N(1,1), \tag{11}$$

where $\rho_N = P_N(1,1) + P_N(0,1)$ is the particle density at the last site. Then using mean-field arguments it can be assumed that

$$P_N(1,1) \approx \rho_{N-1}\rho_N = \rho_{\mathrm{LD}}\rho_N, \tag{12}$$

which leads to

$$J_{\mathrm{exit},N} = \beta\rho_N(1 + (r-1)\rho_{\mathrm{LD}}). \tag{13}$$

The continuity of the current implies that $J_{\mathrm{exit},N} = J_{\mathrm{LD}}$, yielding

$$\rho_N = \frac{J_{\mathrm{LD}}}{\beta\left[1 + (r-1)\rho_{\mathrm{LD}}\right]}. \tag{14}$$

Similar results can be obtained for the HD phase. Here, the exit current is given by [21]

$$J_{\mathrm{HD}} = \beta(y + rx). \tag{15}$$

The stationary condition in the system ($J_{\mathrm{HD}} = J_{\mathrm{bulk}}$) leads to

$$\beta = \frac{(r - C_1)\left[C_1(-r + q(2r-1)) + r(q + r - 2qr + 4(1-q)(q-r)\rho(1-\rho))\right]}{2(q-r)^2(\rho-1)\rho\left[C_1 + r(r - C_1 - 1 + 2(q-r))\right]}. \tag{16}$$

From this expression, we can estimate the bulk density in the HD phase ($\rho_{\mathrm{HD}} = \rho(\beta)$) and the particle flux in this phase. When there are no interactions ($E = 0$), this produces $\rho_{\mathrm{HD}} = 1 - \beta$. For strong repulsions ($E \to -\infty$), we have $\rho_{\mathrm{HD}} = (1-\beta)/(2-\beta)$ [21].

At the entrance, the density deviates from the bulk value and it can be shown that

$$J_{\mathrm{entr},1} = \alpha(1 + (q-1)\rho_{\mathrm{HD}}). \tag{17}$$

Following the same arguments as above, from the stationary condition, $J_{\mathrm{entr},1} = J_{\mathrm{HD}}$, one can evaluate the particle density at the first site as

$$\rho_1 = 1 - \frac{J_{\rm HD}}{\alpha\left[1 + (q-1)\rho_{\rm HD}\right]}. \tag{18}$$

The MC phase is governed by the dynamics in the bulk, and its properties can be found from the condition of the maximal current, $\frac{\partial J_{\rm bulk}}{\partial \rho} = 0$, using equations (4)–(7). The particle density ρ that maximizes the current is the bulk density in the MC phase, $\rho_{\rm MC} = \rho$. The flux in the MC phase $J_{\rm MC}$ is obtained by substituting this density into equation (7). The particle densities at the boundaries deviate from the bulk values, and using the same arguments as above one can obtain

$$\rho_1 = 1 - \frac{J_{\rm MC}}{\alpha\left[1 + (q-1)\rho_{\rm MC}\right]}, \tag{19}$$

and

$$\rho_N = \frac{J_{\rm MC}}{\beta\left[1 + (r-1)\rho_{\rm MC}\right]}. \tag{20}$$

Theoretical analysis using the two-site cluster mean field approach can also determine the location of phase boundaries between different stationary regimes [20, 21]. Substituting $\rho = \rho_{\rm MC}$ in equations (9) and (16), respectively, yields the location of the triple point $\alpha = \alpha_c$ and $\beta = \beta_c$, at which all the three phases coexist in each homogeneous sub-lattice. These parameters are convenient for describing the phase boundaries. It was found that the LD phase exists when $\alpha < \frac{\beta}{\sqrt{q/r}}$ and $\alpha < \alpha_c$, with the parameter α_c being the solution of the relation $\rho_{\rm LD}(\alpha_c) = \rho_{\rm MC}$. Similarly, the HD phase is found for $\alpha > \frac{\beta}{\sqrt{q/r}}$ and $\beta < \beta_c$ with the parameter β_c being the solution of the relation $\rho_{\rm HD}(\beta_c) = \rho_{\rm MC}$. Finally, the MC phase exists for $\alpha \geqslant \alpha_c$ and $\beta \geqslant \beta_c$. For $E = 0$, it can be shown that $\alpha_c = \beta_c = 1/2$, while for strong repulsions ($E \to -\infty$) we obtain $\alpha_c = \beta_c = 1/(1+\sqrt{2})$ [21].

2.3. Coupling homogeneous sub-lattices

We now compute the effective exit rate, $\beta_{\rm eff}$, and the effective entrance rate, $\alpha_{\rm eff}$, for the sub-lattice L_1 and L_2, respectively. The continuity of the particle current in the system implies that the exit current for the sub-lattice L_1 ($J_{{\rm exit},L_1}$), must be equal to the sum of the current flowing out due to the detachment from the site k ($J_{\rm off}$) and the current passing from the site k to the site $k+1$ ($J_{\rm pass}$). Thus, in the steady-state we have

$$J_{{\rm exit},L_1} = J_{\rm off} + J_{\rm pass}. \tag{21}$$

The particle flux due to the dissociation from the site k, depends on the joint occupation status of the sites $k-1$, k and $k+1$, and it can be written as

$$J_{\rm off} = k_{\rm off}\left[P_k(0,1,0) + rP_k(1,1,0) + rP_k(0,1,1) + r^2P_k(1,1,1)\right]. \tag{22}$$

In this expression, functions $P_k(\tau_{k-1}, \tau_k, \tau_{k+1})$ describe the probabilities of finding the particles at the consecutive sites $k-1$, k and $k+1$, where τ_i is an occupation variable associated with any site i. For the occupied sites we have $\tau_i = 1$, and $\tau_i = 0$ for the empty sites. Let us assume that the correlations between occupation of the sites $k-1$, k and $k+1$ are negligible. Then this leads to the simplified expression for the dissociation current,

$$J_{\rm off} = \rho_k k_{\rm off}\left[1 + (r-1)\rho_{k-1}\right]\left[1 + (r-1)\rho_{k+1}\right], \tag{23}$$

where $\rho_{k-1} = \rho_{\text{bulk},L_1}$ and ρ_k and ρ_{k+1} are the last and the first site densities of the sub-lattice L_1 and L_2, respectively.

Because of the nearest-neighbor interactions, the particle current passing from the site k to the site $k+1$ is determined by the occupation status of four consecutive sites, $k-1$, k, $k+1$ and $k+2$. It can be written as

$$J_{\text{pass}} = P_k(0,1,0,0) + rP_k(1,1,0,0) + qP_k(0,1,0,1) + P_k(1,1,0,1). \tag{24}$$

We assume here that the correlations between these sites are negligible, and this produces

$$J_{\text{pass}} = \rho_k(1-\rho_{k+1})\left[(1-\rho_{\text{bulk},L_1})(1+(q-1)\rho_{\text{bulk},L_1}) + \rho_{\text{bulk},L_2}(r+(1-r)\rho_{\text{bulk},L_2})\right]. \tag{25}$$

Using the same mean-field assumptions, the overall exit current from the sub-lattice L_1 can be written as

$$J_{\text{exit},L_1} = \beta_{\text{eff}}\rho_k\left[1+(r-1)\rho_{\text{bulk},L_1}\right]. \tag{26}$$

Substituting equations (23), (25) and (26) into the current continuity relation from equation (21), we obtain the following expression for the effective exit rate from the sub-lattice L_1,

$$\begin{aligned}\beta_{\text{eff}} = {} & k_{\text{off}}(1+(r-1)\rho_{k+1}) + \frac{(1-\rho_{\text{bulk},L_1})(1-\rho_{k+1})(1+(q-1)\rho_{\text{bulk},L_2})}{1+(r-1)\rho_{\text{bulk},L_1}} \\ & + \frac{\rho_{\text{bulk},L_1}(1-\rho_{k+1})(r+(1-r)\rho_{\text{bulk},L_2})}{1+(r-1)\rho_{\text{bulk},L_1}}.\end{aligned} \tag{27}$$

A simpler expression can be obtained for the case $r = \frac{1}{q}$, which corresponds to $\theta = 0.5$ when the interactions equally affect bond-breaking and bond-creating processes. Then we get

$$\beta_{\text{eff}} = k_{\text{off}}\left[1+(r-1)\rho_{k+1}\right] + (1-\rho_{k+1})\left[1+(q-1)\rho_{\text{bulk},L_2}\right]. \tag{28}$$

When there is no inter-molecular interactions, $E = 0$ and $q = r = 1$, we obtain

$$\beta_{\text{eff}} = k_{\text{off}} + 1 - \rho_{k+1}. \tag{29}$$

This agrees with the result that was obtained earlier in [25]. For strong repulsion ($E \to -\infty$), it can be shown that for the general case ($0 < \theta < 1$),

$$\beta_{\text{eff}} = k_{\text{off}} + 1 - 2\rho_{\text{bulk},L_2}. \tag{30}$$

In this limit, we have $q = 0$ and $r \to \infty$, but this expression cannot be obtained by direct substitution of these values into equation (28). Instead, the following arguments can be presented. The flux out of the sub-lattice L_1 at these conditions can only happen from configurations $(0,1,0,0)$ and $(0,1,0,1)$, which correspond to the occupation of sites $k-1$, k, $k+1$ and $k+2$, respectively. This means that if the site k is occupied, $\rho_{k-1} = \rho_{k+1} = 0$ due to strong repulsions. Then we have $J_{\text{exit},L_1} = \beta_{\text{eff}}\rho_k$, $J_{\text{off}} = k_{\text{off}}\rho_k$ and $J_{\text{pass}} = \rho_k P(0,0) = \rho_k(1-P(0,1)-P(1,0)) = \rho_k(1-2\rho_{\text{bulk},L_2})$. Substituting these expressions for the particle fluxes into equation (21) leads to equation (30). This result can also be easily understood by pointing out that the dynamics of interacting monomers in the limit of strong repulsions is identical to the dynamics of dimers (particles occupying two consecutive sites) but without interaction [20, 26].

Similar calculations can be done to evaluate the effective entrance rate, α_{eff}, into the second sub-lattice. The entrance current for the segment L_2 is given by

$$J_{\text{entr},L_2} = \alpha_{\text{eff}}(1+(q-1)\rho_{\text{bulk},L_2}). \tag{31}$$

At the same time, it should be equal to the current that passes from the first segment, $J_{\text{entr},L_2} = J_{\text{pass}}$, from which we derive

$$\alpha_{\text{eff}} = \rho_k(1 - \rho_{\text{bulk},L_1}) + \frac{\rho_k \rho_{\text{bulk},L_1}(r + (1-r)\rho_{\text{bulk},L_2})}{1 + (q-1)\rho_{\text{bulk},L_2}}. \tag{32}$$

A simpler expression for the effective entrance rate can be obtained for the symmetric interactions case, $qr = 1$ ($\theta = 1/2$), which yields

$$\alpha_{\text{eff}} = \rho_k(1 - \rho_{\text{bulk},L_1}) + r\rho_k\rho_{\text{bulk},L_1}. \tag{33}$$

When there is no interactions, $E = 0$, we get

$$\alpha_{\text{eff}} = \rho_k. \tag{34}$$

This result also agrees with what was found earlier [25]. For strong repulsions ($E \to -\infty$) case, it can be shown that

$$\alpha_{\text{eff}} = \rho_k. \tag{35}$$

This is because the only possible configuration for passing at these conditions is $P_{k+1}(1, 0, 0)$, i.e. the site k is occupied, while the sites $k + 1$ and $k + 2$ for the second second segment are empty [26].

2.4. Stationary phase diagrams

Now we can investigate the effect of local dissociations on the phase diagram of interacting particles in our model. Because the dissociation site divides the system into two homogeneous TASEP segments, each of them separately can be found in one of three stationary phases: LD, HD or MC. This suggests that the maximal number of phases in our system is $3 \times 3 = 9$. We use a notation A/B to label them, where A and B describe a phase in the sub-lattice L_1 and L_2, respectively.

However, because of the specific coupling between two sub-lattices not all phases might be materialized in the system. Due to the irreversible dissociation of the particles at the site k, the sub-lattice L_2 can never obtain the MC phase. Even if the sub-lattice L_1 might have the maximal current, it will decrease for the second segment due to the dissociation flux. This removes out the possibility of existence of LD/MC, HD/MC, and MC/MC phases in our system, and it leaves only six possible stationary phases. Let us investigate the conditions for existence of these phases.

2.4.1. MC/HD phase. The MC/HD phase is determined by the following conditions

$$\alpha > \alpha_c, \quad \beta_{\text{eff}} > \beta_c, \tag{36}$$

$$\alpha_{\text{eff}} > \frac{\beta}{\sqrt{q/r}}, \quad \beta < \beta_c, \tag{37}$$

where α_c and β_c are the coordinates of the triple points for homogeneous single-channel interacting TASEP model, as discussed in section 2.2. In addition, the densities at the sites k and $k + 1$ are given by

$$\rho_k = \frac{J_{\text{MC},L_1}}{\beta_{\text{eff}}\left[1 + (r-1)\rho_{\text{MC},L_1}\right]}, \quad \rho_{k+1} = 1 - \frac{J_{\text{HD},L_2}}{\alpha_{\text{eff}}\left[1 + (q-1)\rho_{\text{HD},L_2}\right]}, \tag{38}$$

and they are the functions of α_{eff}, β_{eff} and β. The effective entrance and exit rates are given by

$$\alpha_{\text{eff}} = \rho_k(1-\rho_{\text{MC},L_1}) + \frac{\rho_k\rho_{\text{MC},L_1}\left[r+(1-r)\rho_{\text{HD},L_2}\right]}{1+(q-1)\rho_{\text{HD},L_2}}, \tag{39}$$

and

$$\beta_{\text{eff}} = k_{\text{off}}\left[1+(r-1)\rho_{k+1}\right] + \frac{(1-\rho_{\text{MC},L_1})(1-\rho_{k+1})\left[1+(q-1)\rho_{\text{HD},L_2}\right]}{1+(r-1)\rho_{\text{MC},L_1}} + \frac{\rho_{\text{MC},L_1}(1-\rho_{k+1})\left[r+(1-r)\rho_{\text{HD},L_2}\right]}{1+(r-1)\rho_{\text{MC},L_1}}. \tag{40}$$

For any given values of the interaction energy E, the detachment rate k_{off}, the entrance rate α and the exit rate β, equations (38)–(40) can be solved together numerically by taking into account the explicit expressions for J_{MC}, J_{HD}, ρ_{MC} and ρ_{HD} in terms of α_{eff}, β_{eff} and β. This leads to explicit evaluation of the effective rates α_{eff} and β_{eff} for any set of parameters. Correspondingly, the MC/HD phase can be obtained for the values of α, β, α_{eff}, and β_{eff} satisfying equations (36) and (37).

2.4.2. MC/LD phase. There are following conditions for existence of the MC/LD phase:

$$\alpha > \alpha_c, \quad \beta_{\text{eff}} > \beta_c, \tag{41}$$

$$\alpha_{\text{eff}} < \frac{\beta}{\sqrt{q/r}}, \quad \alpha_{\text{eff}} < \alpha_c. \tag{42}$$

The particle densities at the special sites k and $k+1$ are given as

$$\rho_k = \frac{J_{\text{MC},L_1}}{\beta_{\text{eff}}\left[1+(r-1)\rho_{\text{MC},L_1}\right]}, \quad \rho_{k+1} = \rho_{\text{LD},L_2}(\alpha_{\text{eff}}). \tag{43}$$

For the effective entrance and exit rates we have,

$$\alpha_{\text{eff}} = \rho_k(1-\rho_{\text{MC},L_1}) + \frac{\rho_k\rho_{,L_1}\left[r+(1-r)\rho_{\text{LD},L_2}\right]}{1+(q-1)\rho_{\text{LD},L_2}}, \tag{44}$$

and

$$\beta_{\text{eff}} = k_{\text{off}}(1+(r-1)\rho_{k+1}) + \frac{(1-\rho_{\text{MC},L_1})(1-\rho_{k+1})\left[1+(q-1)\rho_{\text{LD},L_2}\right]}{1+(r-1)\rho_{\text{MC},L_1}} + \frac{\rho_{\text{MC},L_1}(1-\rho_{k+1})\left[r+(1-r)\rho_{\text{LD},L_2}\right]}{1+(r-1)\rho_{\text{MC},L_1}}. \tag{45}$$

Substituting ρ_k and ρ_{k+1} in equations (44) and (45), we get the system of two coupled equations, which can be solved numerically to obtain the effective entrance and exit rates, α_{eff} and β_{eff}. These values are used then to find the parameters range that satisfy the conditions given in equations (41) and (42).

2.4.3. HD/HD phase. This phase exists when

$$\alpha > \frac{\beta_{\text{eff}}}{\sqrt{q/r}}, \quad \beta_{\text{eff}} < \beta_c, \tag{46}$$

$$\alpha_{\text{eff}} > \frac{\beta}{\sqrt{q/r}}, \quad \beta < \beta_c. \tag{47}$$

The densities at the sites k and $k+1$ in this case can be written as

$$\rho_k = \rho_{\text{HD}}(\beta_{\text{eff}}), \quad \rho_{k+1} = 1 - \frac{J_{\text{HD},L_2}}{\alpha_{\text{eff}}\left[1 + (q-1)\rho_{\text{HD},L_2}\right]}. \tag{48}$$

The effective entrance and exit rates are given by

$$\alpha_{\text{eff}} = \rho_k(1 - \rho_{\text{HD},L_1}) + \frac{\rho_k \rho_{\text{HD},L_1}\left[r + (1-r)\rho_{\text{HD},L_2}\right]}{1 + (q-1)\rho_{\text{HD},L_2}}, \tag{49}$$

and

$$\begin{aligned}\beta_{\text{eff}} = k_{\text{off}}(1 + (r-1)\rho_{k+1}) + \frac{(1-\rho_{\text{HD},L_1})(1-\rho_{k+1})\left[1 + (q-1)\rho_{\text{HD},L_2}\right]}{1 + (r-1)\rho_{\text{HD},L_1}} \\ + \frac{\rho_{\text{HD},L_1}(1-\rho_{k+1})\left[r + (1-r)\rho_{\text{HD},L_2}\right]}{1 + (r-1)\rho_{\text{HD},L_1}}.\end{aligned} \tag{50}$$

Substituting expressions for ρ_k and ρ_{k+1} from equation (48)–(50), we derive the system of two coupled equations, which can be numerically solved for α_{eff} and β_{eff} for any particular values of α, β, E and k_{off}. These values are utilized then to evaluate the parameters range for this phase.

2.4.4. LD/HD phase. The LD/HD phase is described by the following conditions,

$$\alpha < \frac{\beta_{\text{eff}}}{\sqrt{q/r}}, \quad \alpha < \alpha_c, \tag{51}$$

$$\alpha_{\text{eff}} > \frac{\beta}{\sqrt{q/r}}, \quad \beta < \beta_c. \tag{52}$$

For this phase, the densities at sites k and $k+1$ are

$$\rho_k = \frac{J_{\text{LD},L_1}}{\beta_{\text{eff}}\left[1 + (r-1)\rho_{\text{LD},L_1}\right]}, \quad \rho_{k+1} = 1 - \frac{J_{\text{HD},L_2}}{\alpha_{\text{eff}}\left[1 + (q-1)\rho_{\text{HD},L_2}\right]}. \tag{53}$$

Moreover, we can write the expressions for the effective entrance and exit rates α_{eff} and β_{eff},

$$\alpha_{\text{eff}} = \rho_k(1 - \rho_{\text{LD},L_1}) + \frac{\rho_k \rho_{\text{LD},L_1}\left[r + (1-r)\rho_{\text{HD},L_2}\right]}{1 + (q-1)\rho_{\text{HD},L_2}}, \tag{54}$$

and

$$\begin{aligned}\beta_{\text{eff}} = k_{\text{off}}(1 + (r-1)\rho_{k+1}) + \frac{(1-\rho_{\text{LD},L_1})(1-\rho_{k+1})\left[1 + (q-1)\rho_{\text{HD},L_2}\right]}{1 + (r-1)\rho_{\text{LD},L_1}} \\ + \frac{\rho_{\text{LD},L_1}(1-\rho_{k+1})\left[r + (1-r)\rho_{\text{HD},L_2}\right]}{1 + (r-1)\rho_{\text{LD},L_1}}.\end{aligned} \tag{55}$$

Utilizing ρ_k and ρ_{k+1} from equations (53) in (54) and (55), we can find numerically exactly the values of the effective entrance and exit rates, α_{eff} and β_{eff}, for any values of E, k_{off}, α and

β. They are used then to determine the boundaries for this phase from conditions presented in equations (51) and (52).

2.4.5. LD/LD phase. The LD/LD phase exists when the parameters α, β, $\alpha_{\rm eff}$, and $\beta_{\rm eff}$ satisfy the following conditions:

$$\alpha < \frac{\beta_{\rm eff}}{\sqrt{q/r}}, \quad \alpha < \alpha_c, \tag{56}$$

$$\alpha_{\rm eff} < \frac{\beta}{\sqrt{q/r}}, \quad \alpha_{\rm eff} < \alpha_c. \tag{57}$$

The densities at the sites k and $k+1$ are given by

$$\rho_k = \frac{J_{{\rm LD},L_1}}{\beta_{\rm eff}\left[1+(r-1)\rho_{{\rm LD},L_1}\right]}, \quad \rho_{k+1} = \rho_{\rm LD}(\alpha_{\rm eff}). \tag{58}$$

Utilizing equations (32) and (27), the effective entrance and exit rates in terms of the bulk densities and densities at the sites k and $k+1$ can be written as

$$\alpha_{\rm eff} = \rho_k(1-\rho_{{\rm LD},L_1}) + \frac{\rho_k\rho_{{\rm LD},L_1}\left[r+(1-r)\rho_{{\rm HD},L_2}\right]}{1+(q-1)\rho_{{\rm HD},L_2}}, \tag{59}$$

and

$$\beta_{\rm eff} = k_{\rm off}\left(1+(r-1)\rho_{k+1}\right) + \frac{(1-\rho_{{\rm LD},L_1})(1-\rho_{k+1})\left[1+(q-1)\rho_{{\rm LD},L_2}\right]}{1+(r-1)\rho_{{\rm LD},L_1}} + \frac{\rho_{{\rm LD},L_1}\left(1-\rho_{k+1}\left[r+(1-r)\rho_{{\rm LD},L_2}\right]\right)}{1+(r-1)\rho_{{\rm LD},L_1}}. \tag{60}$$

Substituting ρ_k and ρ_{k+1}, given by equation (58), in equations (59) and (60), the effective entrance and exit rates, $\alpha_{\rm eff}$ and $\beta_{\rm eff}$, can be explicitly found. Now, using these values in equations (56) and (57), we can determine the region that describes the LD/LD phase in the stationary phase diagram.

2.4.6. HD/LD phase. The HD/LD phase is defined by the following conditions:

$$\alpha > \frac{\beta_{\rm eff}}{\sqrt{q/r}}, \quad \beta_{\rm eff} < \beta_c, \tag{61}$$

$$\alpha_{\rm eff} < \frac{\beta}{\sqrt{q/r}}, \quad \alpha_{\rm eff} < \alpha_c. \tag{62}$$

The densities at the sites k and $k+1$ are given by

$$\rho_k = \rho_{\rm HD}(\beta_{\rm eff}), \quad \rho_{k+1} = \rho_{\rm LD}(\alpha_{\rm eff}). \tag{63}$$

Our explicit calculations did not find any pair of values for the effective entrance and exit rates $(\alpha_{\rm eff}, \beta_{\rm eff})$ that could satisfy the conditions for existence of HD/LD phase. Domain-wall arguments can be invoked here to explain this observation [25, 27]. In this case, two domain walls can be found only near the entrance and near the exit to the system, which suggests that any density gradient at the dissociation site will be unstable in the system. Thus, this phase cannot be found in the TASEP of interacting particles with local dissociations. This brings the

maximal number of possible stationary phases to five phases. But one should also note that depending on the parameters in the system the real number of stationary phases can be less than five, as we will see below.

3. Results and discussions

Since our explicit calculations involve several approximations, theoretical predictions were tested using Monte Carlo computer simulations. Computer simulations were done by considering the lattice with $N = 1000$ sites in order to avoid the finite-size effects due to boundaries. It was assumed also that our system reaches the steady state after 20% of the Monte Carlos steps. The total number of Monte Carlo steps in our simulations was 10^9. Dynamics in the system was analyzed for interaction energies in the range from $-5\ k_{\mathrm{B}}T$ to $+3\ k_{\mathrm{B}}T$, which is considered to be the most relevant for biological molecular motors. Three different values for the energy splitting parameter θ (0, 0.5 and 1) were also utilized. The irreversible dissociation site in all these cases was chosen to be $N/2$.

The results of our theoretical calculations for density profiles for five possible stationary phases are presented in figure 2. Excellent agreement between theoretical predictions and computer simulations is observed in all situations. As one can clearly see, in agreement with our theoretical arguments, the dissociation site divides the system into two homogeneous segments, for which the properties are different.

To better understand the dynamical properties of interacting molecular motors with local dissociations, we calculate stationary phase diagrams for different sets of parameters. The stationary behavior in the system is governed by the parameter θ, interaction energy E and the dissociation rate k_{off}. The results are presented in figures 3–5. It is found that dynamics is influenced by varying the parameter $0 \leqslant \theta \leqslant 1$ (see figure 3), which describes how the processes of bond breaking and bond creation are affected by the interaction. For small and intermediate values of this parameter ($\theta = 0$ and $\theta = 0.5$) only four phases can be realized in the system (figures 3(a) and (b)), and the HD/HD does not exist. For $\theta = 1$ (figure 3(c)), this phase appears and there now five phases in the system. This observation can be explained using the following arguments. The HD phase in the segment L_1 can be achieved only for very small values of the effective exit rate β_{eff}. For the repulsions considered in figure 3 ($E = -1\ k_{\mathrm{B}}T$) we have $r \geqslant 1$, and from equation (50), increasing r will increase β_{eff}, lowering the possibility for the HD phase in the first segment. This is the reason for not observing HD/HD phase for $\theta = 0$ and $\theta = 0.5$. However, for the case $\theta = 1$, we obtain $r = 1$, and the smallest effective exit rates can be achieved, supporting the existence of the HD/HD phase.

One should also notice a very good agreement between theory and computer simulations for $\theta = 1$, while for $\theta = 0$ the agreement is mostly semi-quantitative. The reason for the increasing discrepancy between the theoretical and simulation results is that as we move from $\theta = 1$ to $\theta = 0$, there is the increase in the strength and the range of correlations in the system. The transition rate r is defined in equation (1), and for a fixed negative E the value of r increases from 1 to $\exp(-E)$ (E is given in units of $k_{\mathrm{B}}T$) as θ moves from 1 to 0. The greater the rate r, the faster is the bond breaking process, and this corresponds to stronger and more long-range correlations in the system. Since our theoretical approach employs the two cluster mean-field theory, which accounts only for short-range correlations, the discrepancies between theoretical predictions and computer simulations increase for smaller θ.

The results presented in figure 4 show that interaction energies can also strongly modify the stationary phase diagrams. The number of possible phases can vary drastically depending on the strength and the sign of interactions. For strong repulsions ($E = -5\ k_{\mathrm{B}}T$, figure 4(a)), only

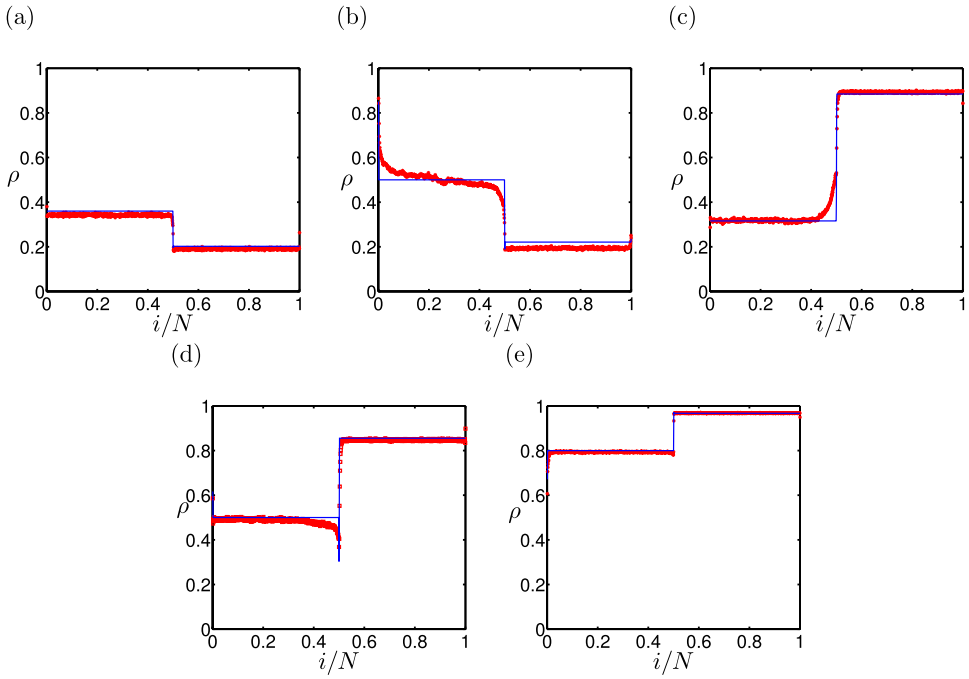

Figure 2. Density profiles for different stationary phases. For all cases, $\theta = 0.5$ and $k_{\text{off}} = 0.3$ were utilized. (a) LD/LD phase for $E = -1$ $k_{\text{B}}T$, $\alpha = 0.5$ and $\beta = 0.5$; (b) MC/LD phase for $E = -1$ $k_{\text{B}}T$, $\alpha = 0.9$ and $\beta = 0.6$; (c) LD/HD phase for $E = +1$ $k_{\text{B}}T$, $\alpha = 0.2$ and $\beta = 0.15$; (d) MC/HD phase for $E = -1$ $k_{\text{B}}T$, $\alpha = 0.95$ and $\beta = 0.1$; (e) HD/HD phase for $E = +1k_{\text{B}}T$, $\alpha = 0.25$ and $\beta = 0.05$. Solid blue lines correspond to numerically exact calculations and red symbols represent the Monte Carlo simulation results.

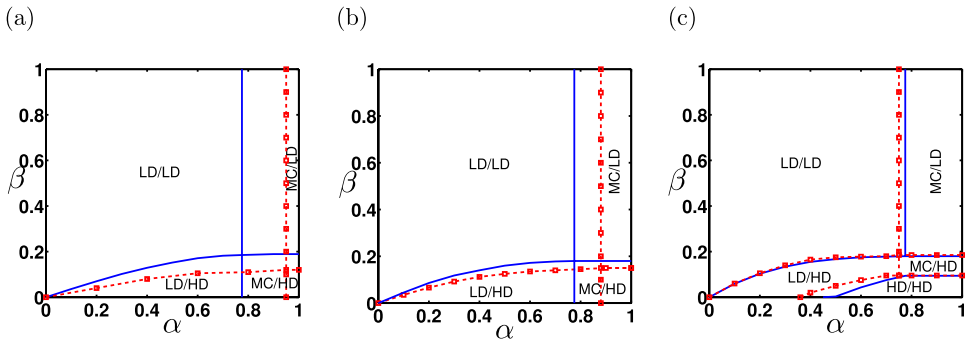

Figure 3. Stationary phase diagrams for $E = -1$ $k_{\text{B}}T$, $k_{\text{off}} = 0.3$ and the splitting parameter (a) $\theta = 0$; (b) $\theta = 0.5$; (c) $\theta = 1$. Solid blue lines correspond to numerically exact calculations and red symbols represent the Monte Carlo simulation results.

two stationary phases are possible for this set of parameters. For these conditions, because of the strong repulsions the HD phase is not possible in both sub-lattices, and the only two phases that can exist are LD/LD and MC/LD. The situation is different for weak repulsions ($E = -1$ $k_{\text{B}}T$, figure 4(b)) when four stationary phases exists. This is because the HD phase is now possible in the sub-lattice L_2, leading to appearance two new LD/HD and MC/HD phases. For

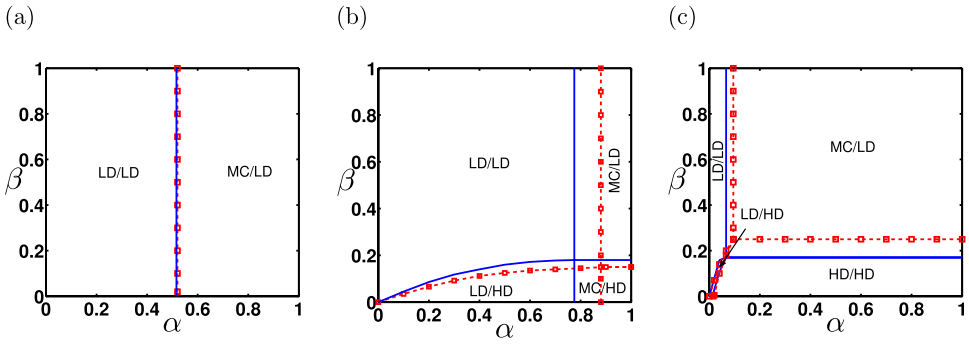

Figure 4. Stationary phase diagrams for varying interaction energies with fixed $\theta = 0.5$ and $k_{\text{off}} = 0.3$: (a) $E = -5\ k_{\text{B}}T$; (b) $E = -1\ k_{\text{B}}T$; (c) $E = 3\ k_{\text{B}}T$. Solid blue lines correspond to numerically exact calculations and red symbols represent the Monte Carlo simulation results.

attractions ($E = +3\ k_{\text{B}}T$, figure 4(c)), we also find four stationary phases, but MC/HD is now substituted by HD/HD phases. In addition, the range for LD/LD and LD/HD is significantly reduced since attractions favor particle clustering, i.e. high-density phases.

Figure 5 shows how the dynamics in the system changes with varying the dissociation rate k_{off}. For parameters considered here (weak repulsions, $E = -1\ k_{\text{B}}T$, and $\theta = 0.5$), there are four stationary phases for the weak dissociation rates: see figure 5(a). Increasing the possibility of the irreversible detachments does not change the number of phases but it modifies one of them: HD/HD phase is substituted by MC/HD phase (figure 5(b)). Increasing further the dissociation rate leads only to changing the phase boundaries without influencing the phase composition (figure 5(c)). These observations can be explained by connecting the dissociation rate with the effective exit rate from the sub-lattice L_1. The larger the detachment rate k_{off}, the larger the rate β_{eff}, which means that the possibility of observing the HD phase in the first segment diminishes. This is the reason for switching HD/HD phase to MC/HD phase: see figures 5(a) and (b).

3.1. Correlations

Analyzing density profiles in different phases, we noticed that our theoretical description in many cases works better for the second sub-lattice than for the first sub-lattice: see figures 2(a) and (d). Because our cluster mean-field method takes into account some correlations in the system, it is reasonable to suggest that the degree of correlations in both segments are not the same. To test this idea, we compute two-point nearest-neighbor correlations in both sub-lattices L_1 and L_2. A general two-point correlation function is defined as

$$C_i = \langle \tau_i, \tau_{i+1} \rangle - \langle \tau_i \rangle \langle \tau_{i+1} \rangle = P(\tau_i = 1, \tau_{i+1} = 1) - P(\tau_i = 1) P(\tau_{i+1} = 1). \tag{64}$$

Since, we treated the sites $k-1$, k, $k+1$, and $k+2$ as independent from each other, the correlations at the sites $k-1$, k and $k+1$ are zero by definition. To maintain the homogeneity in the correlation profiles, we substituted $C_{k-2} = C_{k-1} = C_k$ and $C_{k+1} = C_{k+2}$.

The results of our calculations for correlations in the system are presented in figure 6 for different stationary phases. One can clearly see that in all cases the magnitude of correlations in the second segment is always smaller than the correlations in the first segment, $|C_{L_1}| > |C_{L_2}|$, in agreement with our suggestion. This observation can be explained by the

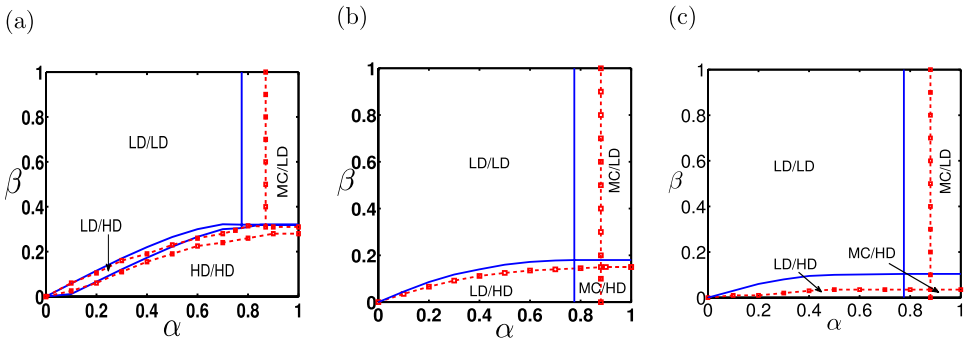

Figure 5. Stationary phase diagrams for varying dissociation rate k_{off} with fixed $\theta = 0.5$ and $E = -1k_{\text{B}}T$: (a) $k_{\text{off}} = 0.03$; (b) $k_{\text{off}} = 0.3$; (c) $k_{\text{off}} = 0.8$. Solid blue lines correspond to numerically exact calculations and red symbols represent the Monte Carlo simulation results.

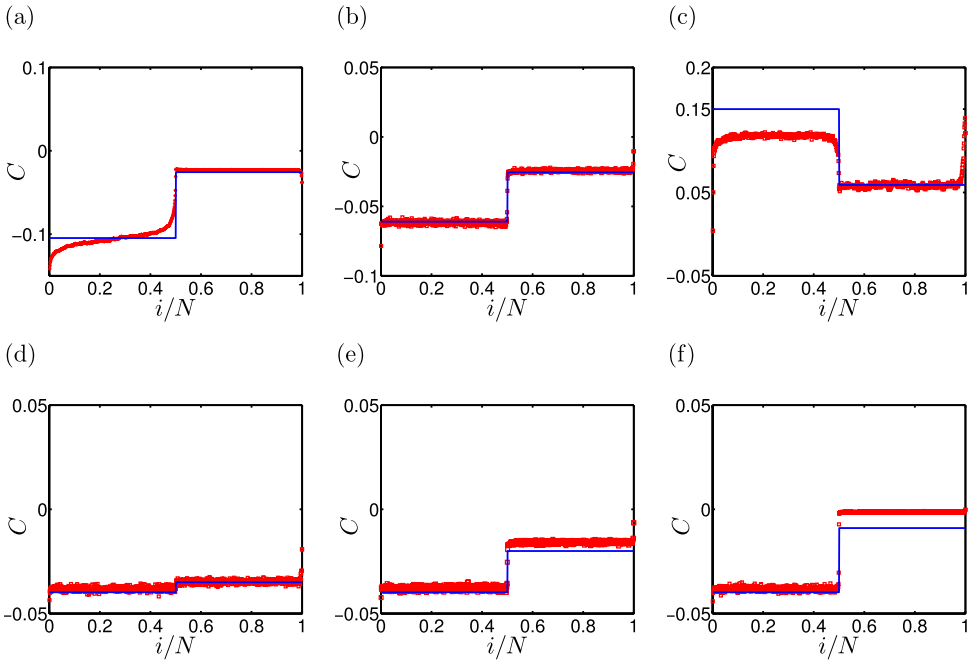

Figure 6. Correlation profiles for the stationary MC/LD phase corresponding to $\alpha = 0.9, \beta = 0.6$, with a fixed $\theta = 0.5$ and E varying as (a) $E = -5\,k_{\text{B}}T$; (b) $E = -1\,k_{\text{B}}T$; (c) $E = 3\,k_{\text{B}}T$. Correlation profiles for the stationary LD/LD phase for $\alpha = 0.4, \beta = 0.4$ with a fixed $E = -1k_{\text{B}}T$, $\theta = 0.5$ and k_{off} varying as (d) $k_{\text{off}} = 0.03$; (e) $k_{\text{off}} = 0.3$; (f) $k_{\text{off}} = 0.8$. Solid blue lines correspond to numerically exact calculations and red symbols represent the Monte Carlo simulation results.

fact that the flux through the second sub-lattice is smaller than the flux via the first sub-lattice because of the flux leaving the system at the dissociation site. The smaller the particle current, the smaller the chance that the probability to find the particle at some site will be affected by the occupation status of the neighboring sites. This corresponds to weaker correlations in the second sub-lattice in comparison with the first sub-lattice.

For repulsive interactions, we observe negative correlations, i.e. $C < 0$: see figures 6(a) and (b). This means that if the given site is occupied the probability to find the particle at the next site is smaller due to being energetically unfavorable. For attractive interactions, the correlations are positive due to increased probability to find the particle at the neighboring site (figure 6(c)). We also investigated the effect of dissociation on the correlations: see figures 6(d)–(f). For the LD/LD phase, it is found that the correlations in the first sub-lattice are independent of k_{off}, while the magnitude of correlations in the second sub-lattice decreases with increasing the dissociation rate. For the LD/LD phase the current in the segment L_1 is fully determined by the entrance rate into the system, and thus it is independent of k_{off}. Consequently, correlations in the first sub-lattice should not depend on the dissociation rate. However, the situation is different for the segment L_2—here the effective entrance rate depends on the dissociation flux. The larger the dissociation rate, the smaller the effective entrance rate α_{eff}. The smaller particle current through the second segment should lead to lower correlations, as we already argued above.

4. Conclusions

We developed a theoretical model for transport of interacting molecular motors with local irreversible dissociations. Our approach is stimulated by experimental observations on protein synthesis by ribosome complexes that move along RNA molecules. It utilizes the TASEP model for interacting particles with the addition of a special site from which the irreversible dissociations are taking place. Although the problem cannot be solved exactly, we present cluster mean-field analytical calculations that describe well the dynamical changes in the system, as was tested with extensive Monte Carlo computer simulations. The main reason for the success of our theoretical method is its ability to capture some of the correlations in the system. In our calculations, we also used the fact that the local dissociation site divides the system into two homogeneous segments for which the explicit analysis can be done. Each of the sub-lattice have its own properties such as density profiles and particle fluxes. It is found that there are up to five possible stationary phases in the system, the boundaries for which are determined by the coupling between the sub-lattices. But the exact number of existing phases varies depending on the parameters. We also show how the strength of inter-molecular interactions, and its splitting on the transition rates and the possibility of irreversible dissociations modify the dynamic features of the system. Microscopic arguments are presented to explain all observed changes. All theoretical predictions are in excellent agreement with results from Monte Carlo computer simulations.

Although our theoretical model is able to explain the complex dynamics of interacting particle with local dissociations, it is important to notice that a more realistic description requires that several other features of the molecular motors transport to be considered. For example, molecular motors typically occupy several sites, they also move with heterogeneous rates determined by the underlying chemical structures of linear tracks (e.g. the sequence dependence of nucleic acids), and there are also conformational fluctuations that lead to variability in the inter-molecular interactions. It will be interesting to investigate the effect of these processes on non-equilibrium dynamics of interacting molecular motors.

Acknowledgments

ABK acknowledges support from the Welch Foundation (Grant C-1559), from the NSF (Grant CHE-1664218) and from the Center for Theoretical and Biological Physics sponsored by the

NSF (Grant PHY-1427654). TM acknowledges DST, Govt. of India and IUSSTF for providing the Indo-US fellowship for women in STEMM, 2018. It was also carried out with the support of CNPq, Conselho Nacional de Desenvolvimento Científico e Tecnológico-Brasil.

ORCID iDs

Arvind Kumar Gupta https://orcid.org/0000-0001-6671-6747
Anatoly B Kolomeisky https://orcid.org/0000-0001-5677-6690

References

[1] Lodish H *et al* 2008 *Molecular Cell Biology* (London: Macmillan)
[2] Phillips R, Theriot J, Kondev J and Garcia H 2012 *Physical Biology of the Cell* (New York: Garland Science)
[3] Kolomeisky A B 2015 *Motor Proteins and Molecular Motors* (Boca Raton, FL: CRC Press)
[4] Kolomeisky A B and Fisher M E 2007 *Annu. Rev. Phys. Chem.* **58** 675–95
[5] Kolomeisky A B 2013 *J. Phys.: Condens. Matter* **25** 463101
[6] Chowdhury D 2013 *Phys. Rep.* **529** 1–197
[7] Bressloff P C and Newby J M 2013 *Rev. Mod. Phys.* **85** 135
[8] Vologodskii A 2006 *Phys. Life Rev.* **3** 119–32
[9] TyleráMcLaughlin R *et al* 2016 *Soft Matter* **12** 14–21
[10] Hancock W O 2014 *Nat. Rev. Mol. Cell Biol.* **15** 615
[11] Roos W H, Campàs O, Montel F, Woehlke G, Spatz J P, Bassereau P and Cappello G 2008 *Phys. Biol.* **5** 046004
[12] Vilfan A, Frey E, Schwabl F, Thormählen M, Song Y H and Mandelkow E 2001 *J. Mol. Biol.* **312** 1011–26
[13] Frank J and Spahn C M 2006 *Rep. Prog. Phys.* **69** 1383
[14] Parmeggiani A, Franosch T and Frey E 2003 *Phys. Rev. Lett.* **90** 086601
[15] Chou T, Mallick K and Zia R 2011 *Rep. Prog. Phys.* **74** 116601
[16] Leduc C, Padberg-Gehle K, Varga V, Helbing D, Diez S and Howard J 2012 *Proc. Natl Acad. Sci.* **109** 6100–5
[17] Golubeva N and Imparato A 2013 *Phys. Rev.* E **88** 012114
[18] Celis-Garza D, Teimouri H and Kolomeisky A B 2015 *J. Stat. Mech.* P04013
[19] Gomes L V and Kolomeisky A B 2017 *J. Phys. A: Math. Theor.* **51** 015601
[20] Midha T, Kolomeisky A B and Gupta A K 2018 *J. Stat. Mech.* 043205
[21] Midha T, Gomes L V, Kolomeisky A B and Gupta A K 2018 *J. Stat. Mech.* 053209
[22] Dierl M, Maass P and Einax M 2012 *Phys. Rev. Lett.* **108** 060603
[23] Dierl M, Einax M and Maass P 2013 *Phys. Rev.* E **87** 062126
[24] Pinkoviezky I and Gov N S 2013 *New J. Phys.* **15** 025009
[25] Mirin N and Kolomeisky A B 2003 *J. Stat. Phys.* **110** 811–23
[26] Yang X Q, Qiu K, Zhang W, Ren L, Xu W T and Deng Y J 2007 *Physica* A **379** 595–606
[27] Kolomeisky A B, Schütz G M, Kolomeisky E B and Straley J P 1998 *J. Phys. A: Math. Gen.* **31** 6911